International Journal of Heat and Mass Transfer 51 (2008) 6180–6193

Contents lists available at ScienceDirect

International Journal of Heat and Mass Transfer

journal homepage: www.elsevier.com/locate/ijhmt

Effect of rear slant angle on flow structures, and pollutant dispersion and concentration fields in the wake of the studied model vehicle

T.L. Chan [a,*], K. Gosse [a], Y. Zhou [a], S.C. Lee [b], X.W. Wang [a], J.F. Huang [a]

[a] Department of Mechanical Engineering, The Hong Kong Polytechnic University, Hung Hom, Kowloon, Hong Kong
[b] Department of Civil and Structural Engineering, The Hong Kong Polytechnic University, Hung Hom, Kowloon, Hong Kong

ARTICLE INFO

Article history:
Received 21 June 2007
Received in revised form 10 May 2008
Available online 4 August 2008

Keywords:
Wind tunnel
Laser Doppler anemometry
Cold wire thermometry
Flow structures
Scalar concentration field
Near-wake
Pollutant dispersion
Vehicular exhaust jet condition

ABSTRACT

Experimental investigations of the interaction effect of rear slant angle (i.e., $\alpha = 25°$ and 60°) and heated air exhaust jet condition (i.e., U_j and T_j) on flow structures, and pollutant (i.e., scalar) dispersion and concentration fields in the near-wake region of two simplified scale-model vehicles at Reynolds number $Re_h = 5.8 \times 10^4$ were performed in a closed-circuit wind tunnel using laser Doppler anemometry (LDA) and the cold wire thermometry. The results show that the behaviors of flow structures and pollutant dispersion in the near-wake region of the studied model vehicles are highly dependent on the interaction effect of U_j/U_∞ and α. For the low value of U_j/U_∞ (i.e., the driving mode from 30 km h^{-1} to 70 km h^{-1}), the wake structure of the two studied model vehicles is almost similar to the case without introducing the vehicular exhaust jet flow, $U_j/U_\infty = 0$, but the scalar concentration is neither sent straight to the wake region nor trapped by the recirculation zone. For higher value of U_j/U_∞ (i.e., the driving mode of 10 km h^{-1}), the jet flow perturbation along the central plane of the vehicular exhaust tailpipe causes the disappearance of the lower vortex in the recirculation zone for the studied model vehicle **A** ($\alpha = 25°$) while it causes the stretching of the recirculation zone for the studied model vehicle **B** ($\alpha = 60°$). The contaminant is mainly straight trajectory along its jet exhaust flow axis. Outside the recirculation zone, the flow field becomes symmetrical and its flow structure depends only on the rear slant angle of the studied model vehicle. The scalar concentration field of the studied model vehicle **B** is characterized by a two-dimensional flow structure whatever the studied driving modes are. The distribution of the mean normalized temperature excess field (i.e., scalar concentration field) conforms to the velocity vector field for both studied model vehicles. For the studied model vehicle **A**, the scalar concentration is drawn to the edge of the trailing vortex at the vehicular exhaust jet side. This phenomenon causes a significant reduction of the scalar concentration level whatever the studied driving modes are.

1. Introduction

Motor vehicle emissions are the major source of air pollution in most urban cities [1]. The exhaust pollutant dispersion from motor vehicles is of particular interest with respect to the improvement of air quality in urban cities. It causes serious impact on urban air quality and public health. Over the decade, the major attention of researchers has mainly been focused on a global approach by the modelling of vehicular exhaust emissions in urban areas such as urban street canyon or near a roadway [2–5]. Pollutant concentration measurements on particle and gaseous emissions have also been performed within a busy urban street canyon [6] and from on-road motor vehicles [7,8].

On the contrary, much less attention has been paid to the studied pollutant in the near-wake region of a ground vehicle. It is vital that the flow structures and pollutant dispersion in the near-wake region of a ground vehicle, and its response to the wind speed and direction be known for short time and distance scales. In general, the interaction between the vehicle wake and vehicular exhaust jet plume dominate the pollutant dispersion which appears by a more or less fast dilution of gaseous/particle emissions in the surrounding medium. These studies not only include the effects of turbulence diffusion, vortex recirculation, heat transfer, dilution and species transport, but also microphysico-chemical processes such as coagulation and chemical reactions [9–14]. This type of pollutant dispersion behaviour not only has direct impact on human health, particularly on the drivers, bicyclists, pedestrians, people working nearby and vehicle passengers [15–17], but also constitutes a major fraction of the total pollutant dispersion [18].

Among these few studies which have tackled scalar dispersion in the vehicle wake, Chan et al. [15] developed a two-dimensional pollutant dispersion numerical model based on the joint-scalar PDF approach and a k–ε turbulence model to simulate the initial

* Corresponding author. Tel.: +852 2766 6656; fax: +852 2365 4703.
E-mail address: mmtlchan@inet.polyu.edu.hk (T.L. Chan).

0017-9310/$ - see front matter © 2008 Elsevier Ltd. All rights reserved.
doi:10.1016/j.ijheatmasstransfer.2008.05.013

Nomenclature

B width of a real on-road vehicle, m
D diameter of a real on-road vehicle exhaust tailpipe, m
H height of a real on-road vehicle, m
I_{ii} turbulent intensity in i component
I_{uvw} total turbulence intensity
$I_{T'_{max}}$ normalized temperature intensity, $I_{T'_{max}} = \sqrt{\overline{T'^{*2}_{max}}}/\overline{T'_{max}}$
L length of a real on-road vehicle, m
Re_j vehicular exhaust jet Reynolds number in Eq. (1)
Re_h Reynolds number, $Re_h = U_\infty h/\nu$
St_p Stokes number, $St_p = \tau_p/\tau_u$
T_j initial temperature excess difference from an exhaust jet, K
T_∞ or T ambient temperature or temperature excess with respect to ambient, K
$\overline{T^*}$ normalized mean temperature excess, $\overline{T^*} = \overline{T}/T_j$
$\sqrt{\overline{T'^{*2}_{max}}}$ normalized maximum standard deviation of the temperature, $\sqrt{\overline{T'^{*2}_{max}}} = \sqrt{\overline{T'^{2}_{max}}}/T_j$
U streamwise velocity in x direction, m s^{-1}
U_j vehicular exhaust jet exit velocity, m s^{-1} in Eq. (2)
$U_{real\ vehicle}$ on-road real vehicle speed, m s^{-1}
U_∞ free stream velocity, m s^{-1}
$\overline{U^*}$ normalized streamwise velocity, $\overline{U^*} = \overline{U}/U_\infty$
$\dot{m}_{j(real\ vehicle)}$ mass flow rate of a vehicular exhaust gas jet from a real on-road vehicle, $\dot{m}_{j(real\ vehicle)} = \rho_{exhaust\ gas} U_{j(real\ vehicle)} \left(\frac{\pi D^2}{4}\right)$, kg s^{-1}
$\dot{m}_{j(model\ vehicle)}$ mass flow rate of a vehicular exhaust hot air jet from a scale-model vehicle, $\dot{m}_{j(model\ vehicle)} = \rho_{hot\ air} U_{j(model\ vehicle)} \left(\frac{\pi d^2}{4}\right)$, kg s^{-1}
$\dot{m}_{real\ vehicle}$ mass flow rate of a real on-road vehicle, $\dot{m}_{real\ vehicle} = \rho_{ambient\ air} U_{real\ vehicle} (BH)_{real\ vehicle}$, kg s^{-1}
$\dot{m}_{model\ vehicle}$ mass flow rate of a scale-model vehicle, $\dot{m}_{model\ vehicle} = \rho_{ambient\ air} U_\infty (bh)_{model\ vehicle}$, kg s^{-1}
b width of a scale-model vehicle, m
d diameter of a scale-model vehicle exhaust tailpipe, m
h height of a scale-model vehicle, m
l length of a scale-model vehicle, m
u relative to the streamwise velocity
v relative to the transversal velocity
w relative to the spanwise velocity
x streamwise coordinate, m
y transverse coordinate, m
z spanwise coordinate, m

Greek symbols
α rear slant angle of scale-model vehicle, °
ρ density, kg m^{-3}
τ_p particle response time, s
τ_u turbulent time scale of the fluid flow, s
ν kinematic viscosity of fluid, m^2 s^{-1}

Other symbols
* dimensionless
$\overline{A}$ mean value of the variable A
rms root mean square

dispersion process of nitrogen oxides, temperature and flow velocity distributions. Wang et al. [17] developed a three-dimensional numerical model based on the Reynolds-averaged Navier-Stokes equations coupled with a k–ε turbulence model to simulate the initial dispersion process of carbon monoxide distributions from a vehicular exhaust plume. This numerical model was validated for the measured data obtained from two types of diesel-fuelled vehicles under both high and low idling conditions. Richards et al. [19] studied numerically and experimentally the influence of the near-wake on pollutant dispersion downstream a fastback model. The numerical simulations of the near-wake flow field and gaseous dispersion were performed using k-ε models. Recently, Dong and Chan [20] and Chan et al. [21] have investigated comprehensively the three-dimensional flow structures and pollutant dispersion (i.e., scalar transport) in the near-wake region of a light-duty diesel vehicle for different rear slant angles (i.e., $\alpha = 25°$ and 60°), stationary (i.e., low and high idling modes) and moving (i.e., vehicle speed mode) vehicle conditions, and ambient wind conditions (i.e., wind speed and direction) within the urban road microenvironment using the large eddy simulation (LES) approach. Gosse et al. [16,22] have studied experimentally the passive scalar diffusion within the near-wake of an Ahmed model [23] (with a rear slant angle of 5°, 25° or 40°) in using heated air injected through a small pipe on one side of the model base. The cold wire thermometry measurements showed that the thermal field is strongly influenced by the rear slant angle. Kanda et al. [24] have recently investigated the dispersion behavior of exhaust gas from a reduced-scale model vehicle (i.e., a passenger car and a small-size truck). The results obtained by the flame ionization detector indicated the two vehicles promoted dispersion in the horizontal and the vertical direction, respectively. The wake field was analyzed by particle image velocimetry (PIV), and the distribution of the mean and the fluctuation flow fields was found to conform with the concentration field of the exhaust gas. However, these recent research works have only studied constant vehicular exhaust jet exit velocity from the vehicle(s) while the actual vehicular exhaust jet exit velocity depends on the real-world on-road vehicle engine/driving condition.

The aim of this paper is intended to study experimentally the interaction effect of vehicular exhaust jet exit condition and the rear slant angle on the flow structures, and pollutant (i.e., scalar) dispersion and concentration fields in the near-wake region of two simplified scale-model vehicles for different rear slant angles (i.e., $\alpha = 25°$ or 60°) and heated air exhaust jet conditions (i.e., U_j and T_j) at Reynolds number $Re_h = 5.8 \times 10^4$.

2. Experimental set-up

Experiments were carried out in a closed circuit wind tunnel with a 2.4-m-long square test section (0.6 m × 0.6 m). The flow uniformity in the test section was about 0.1% and the streamwise turbulence intensity was less than 0.4% in the absence of the studied model vehicle. Two simplified scale-model vehicles **A** and **B** of a rear slant angle for $\alpha = 25°$ and 60°, respectively were used for the present study as shown in Fig. 1 [20,21]. The wake structure of the studied model vehicle **A** ($\alpha = 25°$) is characterized by a three-dimensional flow which is induced by a pair of trailing vortices. The wake structure is much wider than the studied model vehicle **B** ($\alpha = 60°$). Hence, a smaller scale-model vehicle **A** was designed but keeping the same scale-model vehicle ratio in order to minimize the blockage effect of wind tunnel confinement as shown in Fig. 1. Hence, the heights, h, and widths, b of the two studied model vehicles **A** and **B** used were 0.081 and 0.108 m, and 0.09 and 0.12 m, respectively.

The origin of the reference system was located at the rear of the studied model vehicle as shown in Fig. 2b. The x-axis is oriented in

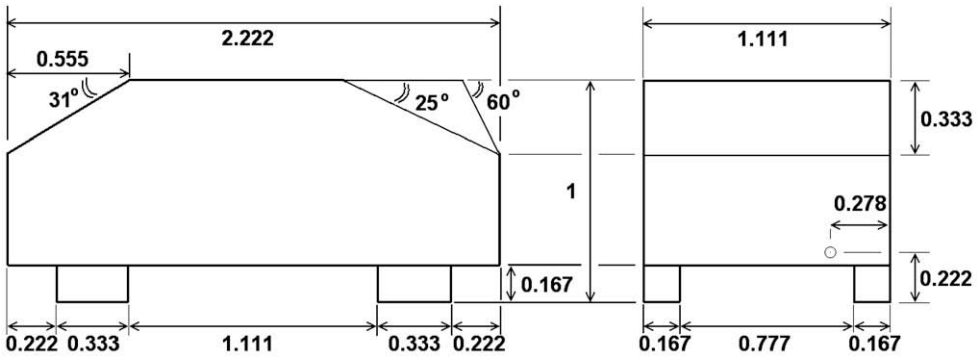

Fig. 1. Two studied scale-model vehicles of rear slant angle, $\alpha = 25°$ (vehicle **A**) and 60° (vehicle **B**) where the dimension is normalized by the vehicle height, $h = 0.081$ m and 0.108 m, respectively.

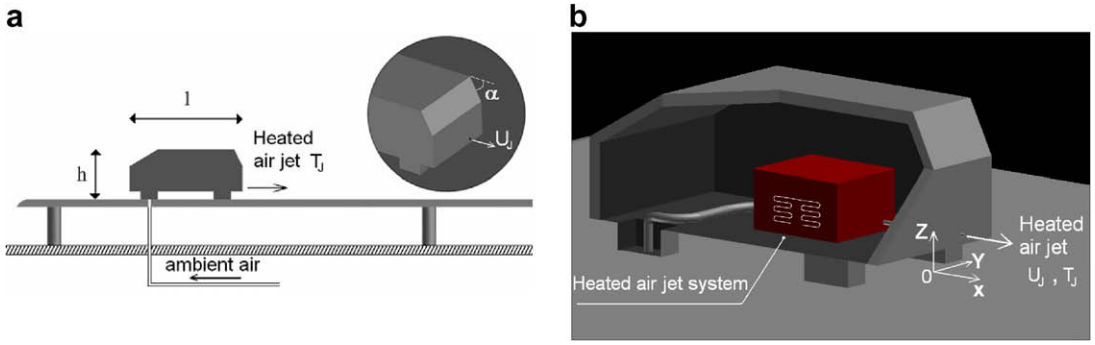

Fig. 2. Wind tunnel study (a) studied model vehicle setup and (b) heated air jet system.

the direction of the main stream flow, U_∞, the y-axis is perpendicular both to the side wall of the studied model vehicle and the main stream flow, and the z-axis is represented to be in the spanwise direction. The studied model vehicle was set on a designed ground plane (2.0 m in length × 0.59 m in width × 0.02 m in thickness) from the wind-tunnel floor as shown in Fig. 2a in order to limit the boundary layer thickness [25]. The details of boundary layer thickness and rms values of this designed flat plate can be referred to Huang et al. [26]. Measurements were performed for two different studied model vehicles **A** and **B** at the free-stream velocity, U_∞ in order to obtain the Reynolds number, $Re_h = 5.8 \times 10^4$.

The vehicular exhaust tailpipe pollutant concentration of on-road vehicle was simulated using a heated air jet at certain temperature T_j and velocity U_j through a small tailpipe exit of diameter $d = 2 \times 10^{-3}$ m and 3×10^{-3} m for two different studied scale-model vehicles **A** and **B**, respectively. The exhaust tailpipe exit was located at the back side of the studied model vehicle (i.e., $x/h = 0$, $y/h = 0.278$, $z/h = 0.22$) as shown in Fig. 1. In order to avoid the possible perturbation of the flow by the heated air injection system, the ambient air tube was inserted through the left front tire of the studied model vehicle and connected to the heating element device and produced the necessary hot air jet exit condition as shown in Fig. 2b. The temperature difference between the potential core of the heated air jet, T_j and the ambient air, T_∞ was maintained constantly at 30 °C using a dedicated temperature feedback control system [27]. The heating element device was placed inside the studied model vehicle as shown in Fig. 2b. The studied parameters of the studied model vehicle conditions were summarized in Table 1, which shows the exit conditions of a vehicular exhaust tailpipe from a typical on-road light-duty diesel vehicle of the exhaust tailpipe diameter, $D = 0.054$ m for different driving modes.

Table 1
Exit conditions from a vehicular exhaust tailpipe of a typical on-road light-duty vehicle [8,21]

Driving mode	$T_{j(\text{real vehicle})}$(K)	$U_{j(\text{real vehicle})}$ (m s^{-1})
10 km h^{-1}	371.9	7.7
30 km h^{-1}	395.1	8.1
50 km h^{-1}	419.2	13.9
70 km h^{-1}	473.0	17.1

In order to study the effect of the vehicular exhaust tailpipe exit conditions for different driving modes, the experiments were performed based on the different exhaust gas flow rates from these two studied scale-model vehicle models **A** and **B**. As described by Kanda et al. [24], the exit jet velocity, U_j could not be directly linked to its Reynolds number:

$$Re_j = \frac{U_{j(\text{real vehicle})} \times D}{\nu_{\text{exhaust gas}}} = \frac{U_{j(\text{model vehicle})} \times d}{\nu_{\text{hot air}}}, \tag{1}$$

$$U_{j(\text{model model})} = \frac{\nu_{\text{hot air}}}{\nu_{\text{exhaust gas}}} \left(\frac{D}{d}\right) U_{j(\text{real vehicle})}. \tag{2}$$

For example, if the driving mode of a real world on-road vehicle is 30 km h^{-1}, then the respective vehicular tailpipe exit jet velocity for the studied scale-model vehicle **B** ($\alpha = 60°$) would be equal to $U_{j_{(\text{model vehicle})}} = 98$ m s^{-1}.

The exit jet velocity, U_j of the scale-model was then determined by the conservation of the mass flow rates from the vehicular exhaust tailpipe conditions of the real and scale-model vehicles in Eq. (3) as follows:

$$\frac{\dot{m}_{j(\text{real vehicle})}}{\dot{m}_{\text{real vehicle}}} = \frac{\dot{m}_{j_{(\text{model vehicle})}}}{\dot{m}_{\text{model vehicle}}}, \tag{3}$$

Table 2
Parameters based on the studied scale-model vehicles

Driving mode	$\dot{m}_{j(\text{real vehicle})}/\dot{m}_{\text{real vehicle}}$	$U_{j(\text{model vehicle})}/U_\infty$	
		Vehicle **A** ($\alpha = 25°$)	Vehicle **B** ($\alpha = 60°$)
10 km h^{-1}	1.802×10^{-3}	4.395	2.813
30 km h^{-1}	5.950×10^{-4}	1.452	0.929
50 km h^{-1}	5.768×10^{-4}	1.407	0.901
70 km h^{-1}	4.484×10^{-4}	1.094	0.701

$$\text{thus} \quad \frac{\rho_{\text{exhaust gas}} U_{j(\text{real vehicle})} \left(\frac{\pi D^2}{4}\right)}{\rho_{\text{ambient air}} U_{\text{real vehicle}} (\text{BH})_{\text{real vehicle}}} = \frac{\rho_{\text{hot air}} U_{j(\text{model vehicle})} \left(\frac{\pi d^2}{4}\right)}{\rho_{\text{ambient air}} U_\infty (\text{bh})_{\text{model vehicle}}}. \tag{4}$$

Finally, the ratio U_j/U_∞ of the scale-model vehicle can then be expressed as:

$$\frac{U_{j(\text{model vehicle})}}{U_\infty} = \frac{(\text{bh})_{\text{model vehicle}}}{(\text{BH})_{\text{real vehicle}}} \frac{U_{j(\text{real vehicle})}}{U_{\text{real vehicle}}} \times \frac{\rho_{\text{exhaust gas}}}{\rho_{\text{hot air}}} \times \frac{D^2}{d^2}, \tag{5}$$

where the kinematic viscosity, $v_{\text{exhaust gas}}$ and density of the exhaust gas, $\rho_{\text{exhaust gas}}$ are then determined from Silva et al. [28], and the height, H and width, B of a typical on-road light-duty diesel vehicle 1.8 m and 2.0 m, respectively.

The parameters of the studied model vehicle conditions were summarized in Table 2. Since the ratios of $\dot{m}_{j(\text{real vehicle})}/\dot{m}_{\text{real vehicle}}$ and U_j/U_∞ for the driving modes at 30 and 50 km h^{-1} are quite similar, only the driving modes of 10, 30, 70 km h^{-1} were used for the present study.

Laser Doppler Anemometry (LDA) (Dantec Model 58N40) with an enhanced flow velocity analyzer (FVA) signal processor was used to measure and analyze their mean velocity, $\overline{U}$, $\overline{V}$ and $\overline{W}$ and root mean square, u_{rms}, v_{rms}, w_{rms} components of the three-dimensional flow and turbulence fields in the wake of the studied model vehicles. The flow was seeded by smoke generated from paraffin oil with the averaged particle size of around 1 μm in diameter. The measuring volume of the LDA system has a minor axis of 1.18 mm and a major axis of 2.48 mm. Each data point has an average of more than 5000 instantaneous samples.

A cold wire anemometry was used to measure instantaneous temperature excess in the near-wake region of the studied model vehicle. The fine cold-wire has made of 1.27 μm diameter Wollaston (Pt-10% Rh) wire with a current of 0.1 mA. The frequency response of this temperature probe is about 2 kHz. Signals from the circuits are offset, amplified and then digitized using a 16 channel (12 bit) A/D board and a personal computer at a sampling frequency of 5 kHz. The duration of each sampling time is 10 s [29].

3. Results and discussion

Fig. 3 shows the cross-sectional x–z plane of the time-averaged flow streamlines for the two studied model vehicles at $y/h = 0$ with $U_j = 0$. For the studied model vehicle **B** ($\alpha = 60°$), the flow is detached above its rear slant angle to form a pair of counter-rotary vortices which is located from the back side to the rear slant angle of model vehicle. The length of the recirculation is obtained at about $x/h = 0.98$. Beyond this recirculation zone, the flow streamlines are practically parallel to the ground. For the studied model vehicle **A** ($\alpha = 25°$), a boundary layer is created above its rear slant angle. The length of the recirculation zone is much shorter at about $x/h = 0.64$ and the flow streamlines are directed towards the ground. These flow behaviors for different rear slant angles $\alpha = 25°$ and 60° are in agreement with the results of Ahmed [30]

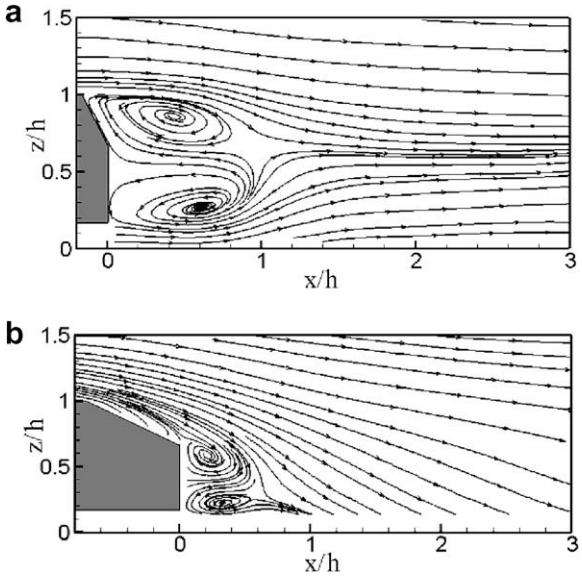

Fig. 3. Time-averaged flow streamlines of the studied model vehicles at the cross-section plane x–z at $y/h = 0$ for rear slant angle (a) $\alpha = 60°$ (vehicle **B**) and (b) $\alpha = 25°$ (vehicle **A**).

for the effect of the rear slant angle on the flow structure in the near-wake of a simplified model vehicle.

Fig. 4 shows the time-averaged velocity vectors and the normalized streamwise velocity, $\overline{U^*}$ contours of the back side of the studied model vehicles **A** and **B** at $x/h = 0$ without introducing the vehicular exhaust jet. The three-dimensional flow behavior of the studied model vehicle **A** is characterized by the creation of a pair of two longitudinal vortices at the edges of the rear part of studied model vehicle as shown in Fig. 4a. Comparing with Figs. 4a and b, it confirms on the contrary the two-dimensional flow configuration of the studied model vehicle B ($\alpha = 60°$) by the lack of longitudinal vortices, and the presence of the recirculation zone is above the rear slant angle from the negative values of $\overline{U^*}$.

Figs. 5 and 6 show the time-averaged flow streamlines in the central plane of the vehicular exhaust tailpipe of two studied model vehicles **B** and **A**, respectively which are used to simulate the variation of vehicular exhaust jet exit, U_j condition in respect to their corresponding driving modes. For the studied model vehicle **B**, their flow behaviors are quite similar when the value of the ratio U_j/U_∞ is equal to 0 to 0.929. However, the shape of the recirculation zone seems to be more stretched when U_j/U_∞ is getting higher (i.e., the driving mode is equal to 10 km h^{-1}) as shown in Fig. 5b. The length of the recirculation zone is about $x/h = 0.82$ as shown in Fig. 5b whereas for the lower values of exhaust jet velocity (i.e., $0 \leqslant U_j/U_\infty \leqslant 0.93$), this length is shorter at about $x/h = 0.72$. For the studied model vehicle **A**, there is not much difference observed except for the driving mode of 10 km h^{-1} case as shown in Fig. 6b. The lower vortex of the recirculation zone disappeared when $U_j/U_\infty = 4.395$. However, the position of the upper bubble vortex is similar to the other cases as shown in Fig. 6. The studied model vehicle **A** is more affected by the condition of the vehicular exhaust jet exit as shown in Fig. 6b in particular close to the injection zone. Two reasons can explain the different flow field behaviors for the driving mode of 10 km h^{-1} case. For the studied model vehicle **B** in the recirculation zone, the lower vortex is about twice larger than the three-dimensional flow field case for the studied model vehicle **A**. This vortex would be also less sensitive to the influence of the vehicular exhaust jet.

Figs. 7 and 8 show the time-averaged velocity vectors and the normalized streamwise velocity $\overline{U^*}$ contours of the driving mode

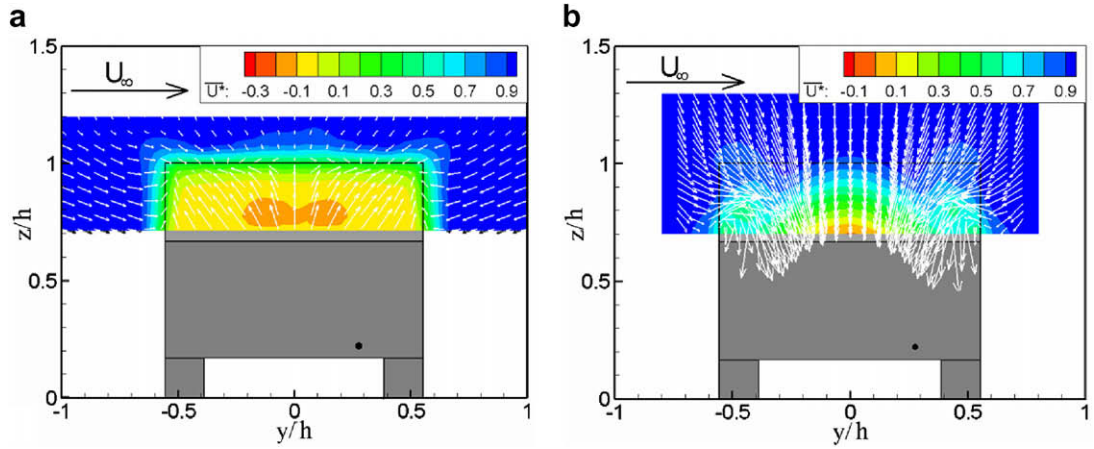

Fig. 4. Time-averaged velocity vectors and normalized streamwise velocity, $\overline{U^*}$ contours of the studied model vehicles at the cross-section plane, z–y at $x/h = 0$ for (a) α=60° (vehicle **B**) and (b) $\alpha = 25°$ (vehicle **A**).

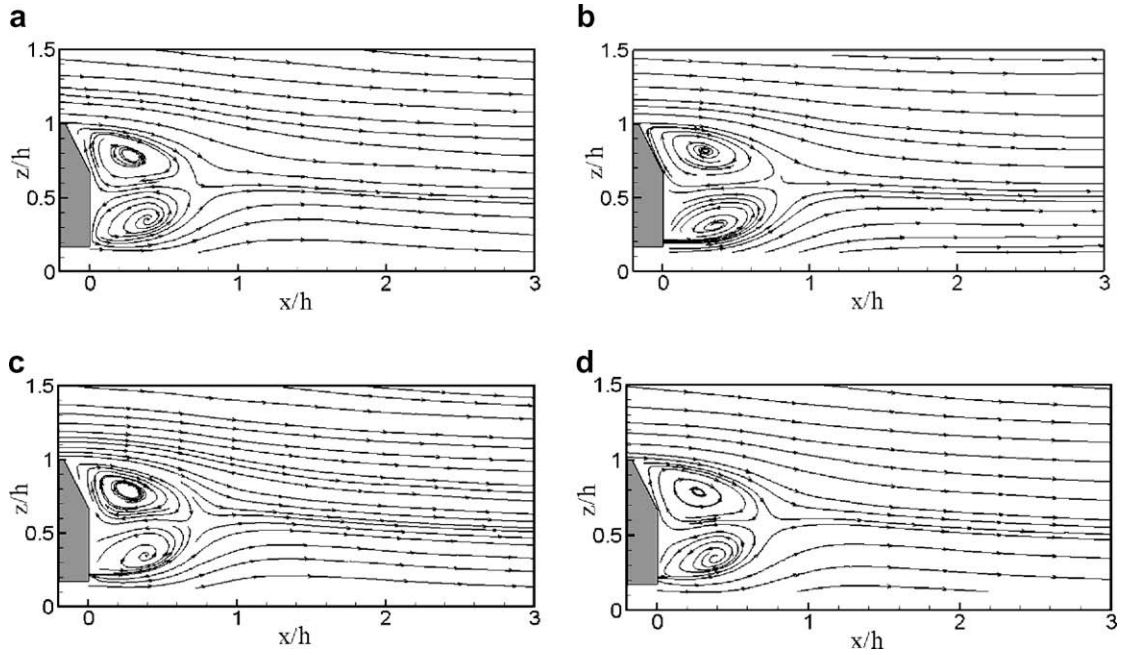

Fig. 5. Time-averaged flow streamlines of the studied model vehicle **B** ($\alpha = 60°$) in the cross-section plane x–z at $y/h = 0.278$ (i.e., the central plane of vehicular exhaust tailpipe exit) for (a) $U_j/U_\infty = 0$, (b) $U_j/U_\infty = 2.813$, (c) $U_j/U_\infty = 0.929$ and (d) $U_j/U_\infty = 0.701$.

of 10 km h^{-1} for the studied model vehicles **B** and **A** at $x/h = 0.125$, 0.5, 1 and 2, respectively. The results reveal that the two-dimensional flow field developed along the downstream of the studied model vehicle **B** as shown in Fig. 7. At $x/h = 0.125$ (i.e., the closest distance from the back side of studied model vehicle), the effect of the vehicular jet plume is only limited to the closer region near the location of exhaust tailpipe. The flow field is still practically symmetrical to the centreline of the studied model vehicle **B** at $y/h = 0$. From $x/h = 0.5$ to 2, the velocity vectors mainly converge to the minimal streamwise velocity area. However, this area is slightly decentred which causes an asymmetry of the velocity vector field. At $x/h = 2$, the flow field becomes symmetrical again and the velocity vectors converge to the streamwise velocity in deficit zone close to the ground at the centerline of the studied model vehicle **B**, $y/h = 0$. The three-dimensional flow field in the counter-rotating trailing vortices is developed along the downstream of studied model vehicle **A** as shown in Fig. 8. These results agree well with the findings in Fig. 6b. From $x/h = 0.125$ to 0.5, the vehicular exhaust jet plume creates a local perturbation of the velocity field in a region close to its injection zone. Between $x/h = 0.125$ and $x/h = 0.5$, the maximum streamwise velocity area is located close to the movement of exhaust jet plume laterally. This slight translatory movement is underlined by the direction of velocity vectors close to its injection zone at $x/h = 0.125$. From $x/h = 1$ to 2, the flow field is symmetrical to the centerline of studied model vehicle **A** at $y/h = 0$ and the cores of the longitudinal vortices move vertically to the ground. At $x/h = 2$, the trailing vortices region is distinguished by a deficit of the streamwise velocity. For low value of U_j/U_∞ (i.e., their corresponding driving modes from 30 to 70 km h^{-1}), its flow structure field is similar to the results without introducing the vehicular exhaust jet flow in the wake structure as shown in Figs. 5 and 6. However, the flow structure becomes more perturbed and asymmetrical when its corresponding driving mode is 10 km h^{-1} as shown in Figs. 7 and 8b. The vehicular jet flow is further developed and modifies the local structure of the recirculation zone.

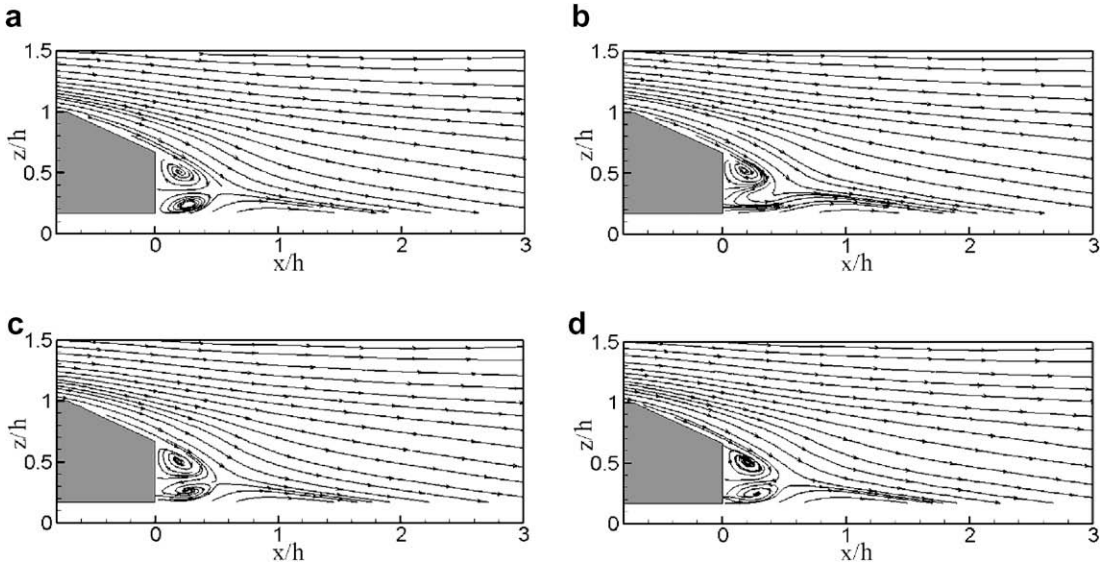

Fig. 6. Time-averaged flow streamlines of the studied model vehicle **A** ($\alpha = 25°$) in the cross-section plane x–z at $y/h = 0.278$ (i.e., the central plane of vehicular exhaust tailpipe exit) for (a) $U_j/U_\infty = 0$, (b) $U_j/U_\infty = 4.395$, (c) $U_j/U_\infty = 1.452$ and (d) $U_j/U_\infty = 1.094$.

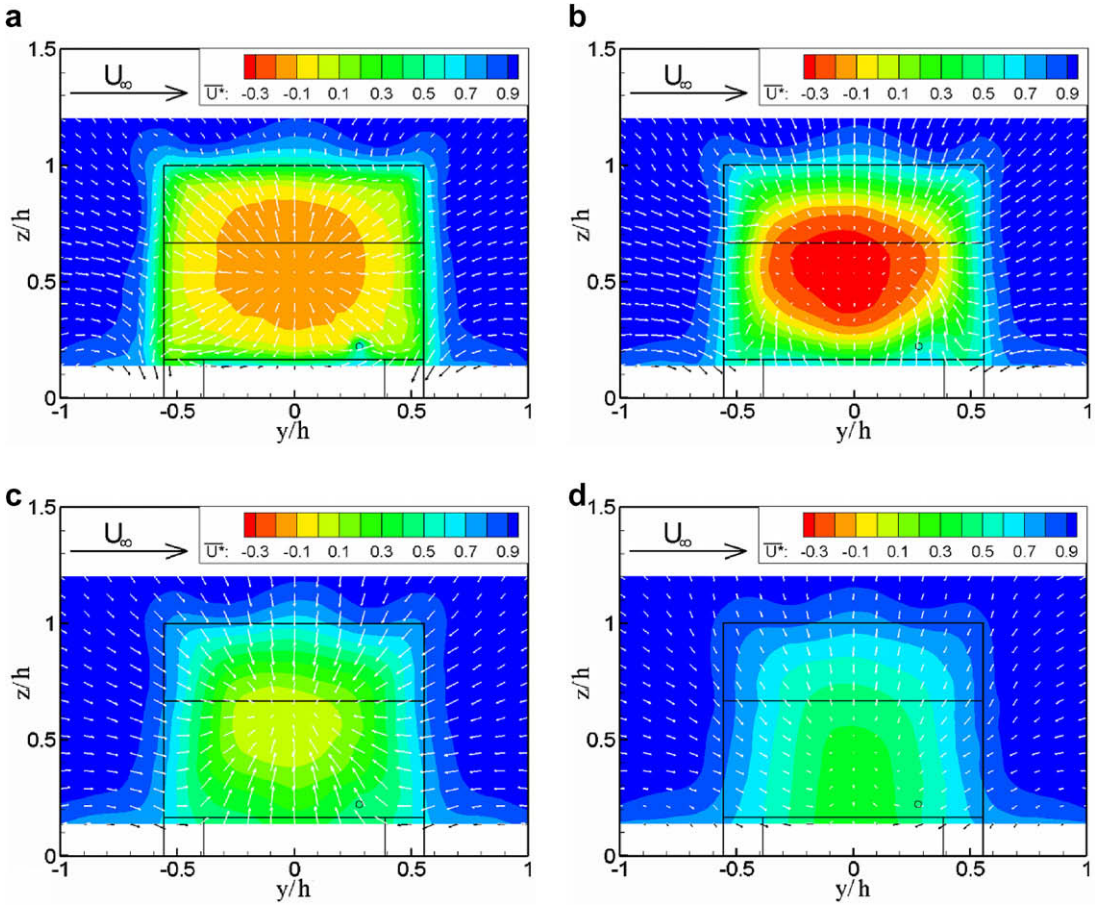

Fig. 7. Time-averaged velocity vectors and normalized streamwise velocity, $\overline{U^*}$ contours of the studied model vehicle **B** ($\alpha = 60°$) for $U_j/U_\infty = 2.813$ at (a) $x/h = 0.125$, (b) $x/h = 0.5$, (c) $x/h = 1$ and (d) $x/h = 2$.

Figs. 9 and 10 show the velocity fields obtained from two different rear slant angles of the studied model vehicles **B** and **A** at $x/h = 0.125$ and 0.5 for the driving mode of 30 km h^{-1}. The flow field is slightly perturbed at $x/h = 0.125$, in particular for the studied model vehicle **A** as shown in Fig. 10a. At $x/h = 0.5$, the flow field becomes symmetrical to the centreline of the studied model vehicle at $y/h = 0$ whatever the geometry of studied vehicle is. Beyond $x/h = 0.5$, the results show a similar flow field behavior whatever the value of U_j/U_∞ or the geometry of the studied model vehicle are. Figs. 5–10 demonstrate clearly for

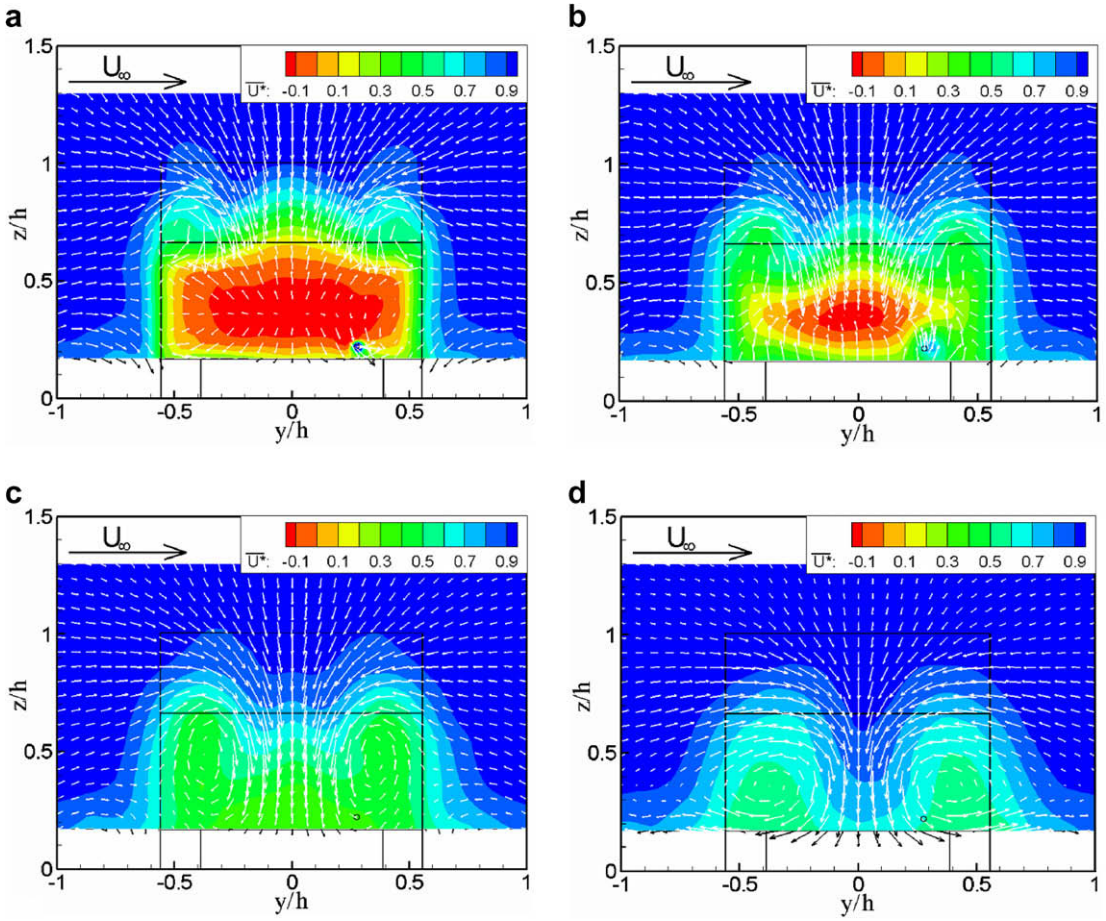

Fig. 8. Time-averaged velocity vectors and normalized streamwise velocity, $\overline{U^*}$ contours of the studied model vehicle **A** ($\alpha = 25°$) for $U_j/U_\infty = 4.395$ at (a) $x/h = 0.125$, (b) $x/h = 0.5$, (c) $x/h = 1$ and (d) $x/h = 2$.

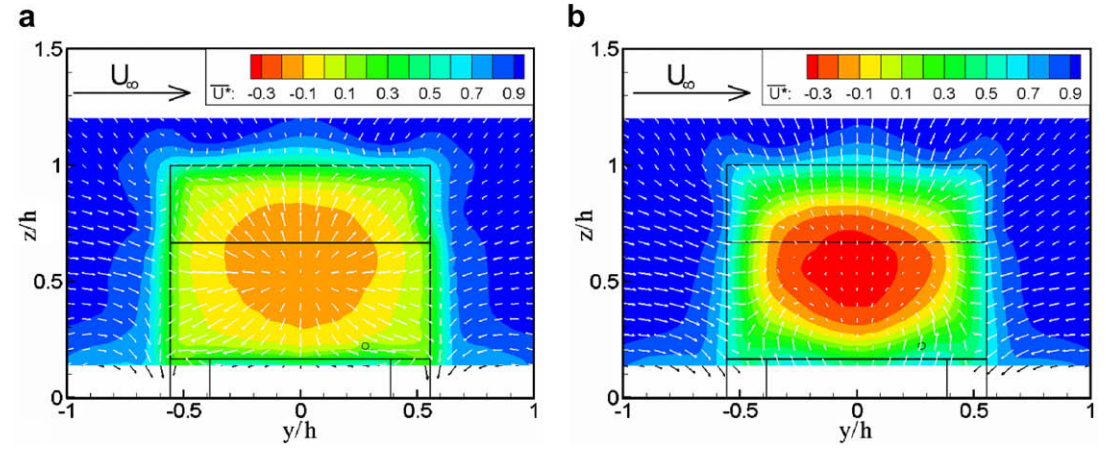

Fig. 9. Time-averaged velocity vectors and normalized streamwise velocity contours of the studied model vehicle **B** ($\alpha = 60°$) for $U_j/U_\infty = 0.929$ at (a) $x/h = 0.125$ and (b) $x/h = 0.5$.

the first time that the flow field reveals the creation of a local flow perturbation in the vicinity of the vehicular exhaust tailpipe whatever the geometry of the studied model vehicle or the jet exit velocity is. Outside the recirculation zone, the flow field recovers in two- or three-dimensional flow behavior in respect to the rear slant angle, α of the studied model vehicles **B** ($\alpha = 60°$) or **A** ($\alpha = 25°$), respectively. In the present study, the results agree well with the previous studies of the simplified model vehicles [23,31,32].

The results also demonstrate that the studied model vehicle **A** is most sensitive to the effect of the vehicular exhaust jet. In order to have a better understanding of the interaction effect of the variation of vehicular exhaust jet exit, U_j and rear slant angle, α in the wake structure region, the turbulence intensity distributions of its right half-plane (i.e., $y/h > 0$) of the studied model vehicle at $x/h = 0.125$, 0.5 and 1 when $U_j/U_\infty = 0$, 4.395 and 1.452 are shown in Figs. 11–13. Turbulence intensity, I_{uvw} and its components, I_{ii} are expressed as:

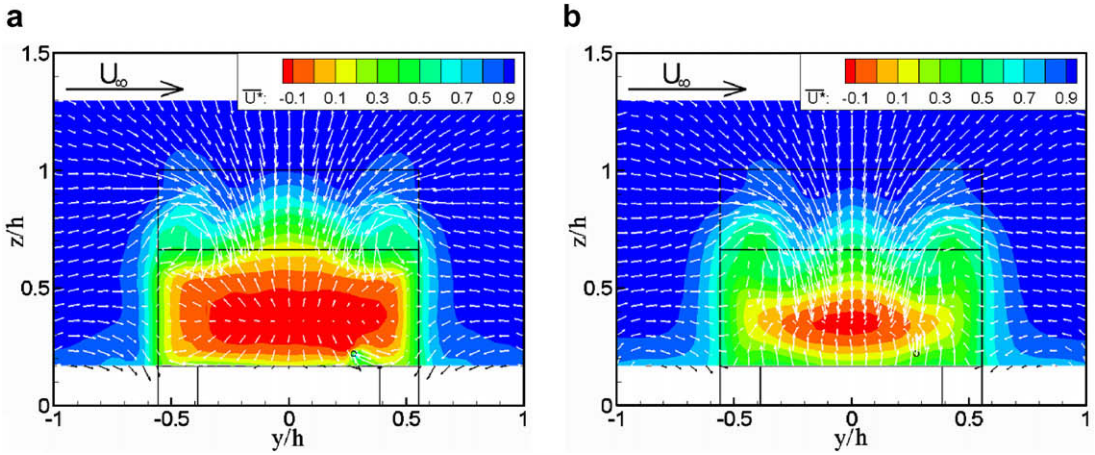

Fig. 10. Time-averaged velocity vectors and normalized streamwise velocity, $\overline{U^*}$ contours of the studied model vehicle **A** ($\alpha = 25°$) for $U_j/U_\infty = 1.452$ at (a) $x/h = 0.125$ and (b) $x/h = 0.5$.

$$I_{uvw} = \sqrt{\frac{I_{uu}^2 + I_{vv}^2 + I_{ww}^2}{3}} \quad \text{and} \quad I_{ii} = \frac{\sqrt{\overline{i'^2}}}{U_\infty} = \frac{i_{rms}}{U_\infty}$$
$$\text{where} \quad i = u, v \quad \text{or} \quad w. \tag{6}$$

In Fig. 11a, the maximum value of I_{uvw} of the studied model vehicle A is located close to the lateral edge of the recirculation zone (i.e., $y/h = 0.555$) while the core of the trailing vortex is located at around $0.25 \leqslant y/h \leqslant 0.50$ and $0.62 \leqslant z/h \leqslant 0.80$ for $x/h = 0.125$ and $U_j/U_\infty = 0$ case. In Fig. 11b, the maximum value of I_{uvw} is located at the centre of the wake structure and close to the end of the bubble zone while its longitudinal eddy is located at around $0 \leqslant y/h \leqslant 0.555$ and $0.167 \leqslant z/h \leqslant 0.6$ for $x/h = 0.5$ and $U_j/U_\infty = 0$ case. In Fig. 11c, the maximum value of I_{uvw} coincides with the position of the trailing vortex which is located at around $0.30 \leqslant y/h \leqslant 0.60$ and $0.20 \leqslant z/h \leqslant 0.80$ for $x/h = 1$ and $U_j/U_\infty = 0$ case. In Figs. 12a and b, the maximum values of I_{uvw} of the studied model vehicle **A** are located at the front of its exhaust tailpipe exit and reached to $I_{uvw,\,max} = 0.6$ and $I_{uvw,\,max} = 0.26$ at $x/h = 0.125$ and $x/h = 0.5$, respectively for $U_j/U_\infty = 4.395$ case. Comparing with Figs. 11b and 13b, the similar I_{uvw} contours of the studied model vehicle **A** are obtained at $x/h = 0.5$ for $U_j/U_\infty = 0$ and $U_j/U_\infty = 1.452$, respectively. Close to the injection zone at $x/h = 0.125$, the maximum value of I_{uvw} is equal to 0.31 in Fig. 13a. Beyond $x/h \geqslant 0.125$, the values of I_{uvw} are similar to the case of $U_j/U_\infty = 0$ in Figs. 13b and c.

Figs. 12 and 13, the results of the turbulence intensity underlines the similar behaviors obtained from the results of the mean flow fields in Figs. 8 and 10. Whatever the driving mode (i.e., 10 to 70 km h^{-1}) is used, the presence of a local jet flow perturbation is more or less unsteady flow according to the value of U_j/U_∞ in the vicinity of the vehicular exhaust tailpipe exit at $x/h = 0.125$ as shown in Figs. 12 and 13a. For low value of U_j/U_∞ (i.e., driving modes from 30 to 70 km h^{-1}) at $x/h = 0.5$, the unsteady behavior in the wake structure does not depend on the jet flow effect as shown in Fig. 13b. The flow structure field becomes similar to the results obtained for $U_j/U_\infty = 0$ case as shown in Fig. 11. In Fig. 12b, the high value of $U_j/U_\infty = 4.395$ (i.e., driving mode of 10 km h^{-1}) at $x/h = 0.5$ case, the development of the exhaust jet flow contributes to the increasing the size of unsteady flow area near its exhaust tailpipe exit of the studied model vehicle **A**. Beyond $x/h = 0.5$, the wake structure of the studied model vehicle does not change whatever the value of U_j/U_∞ is and the turbulence intensity levels are similar to the case of $U_j/U_\infty = 0$.

In the present study, the slightly heated air jet (i.e., a tracer gas) was used to simulate a neutrally hot air buoyant effluent, and their temperature (i.e. scalar concentration) and flow fields behind the

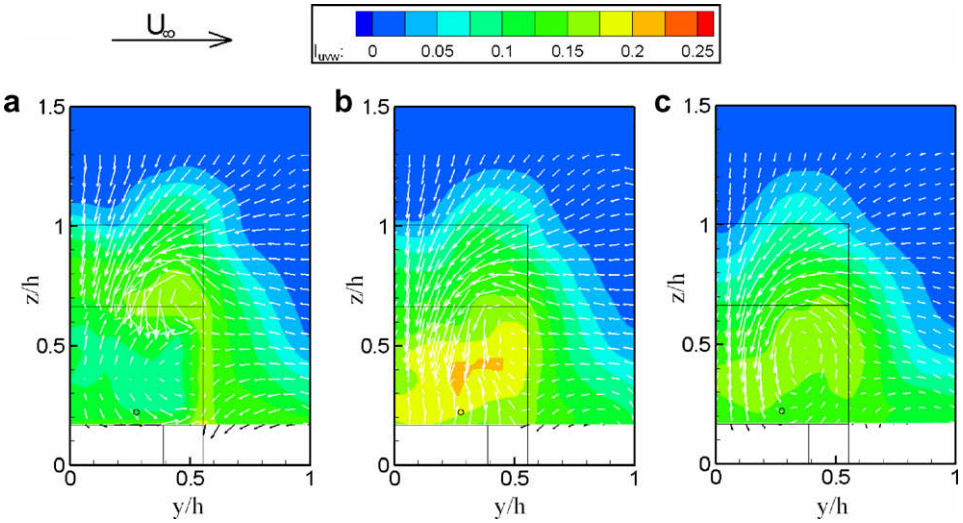

Fig. 11. Turbulence intensity, I_{uvw} contours of the studied model vehicle **A** ($\alpha = 25°$) for $U_j/U_\infty = 0$ at (a) $x/h = 0.125$, (b) $x/h = 0.5$ and (c) $x/h = 1$.

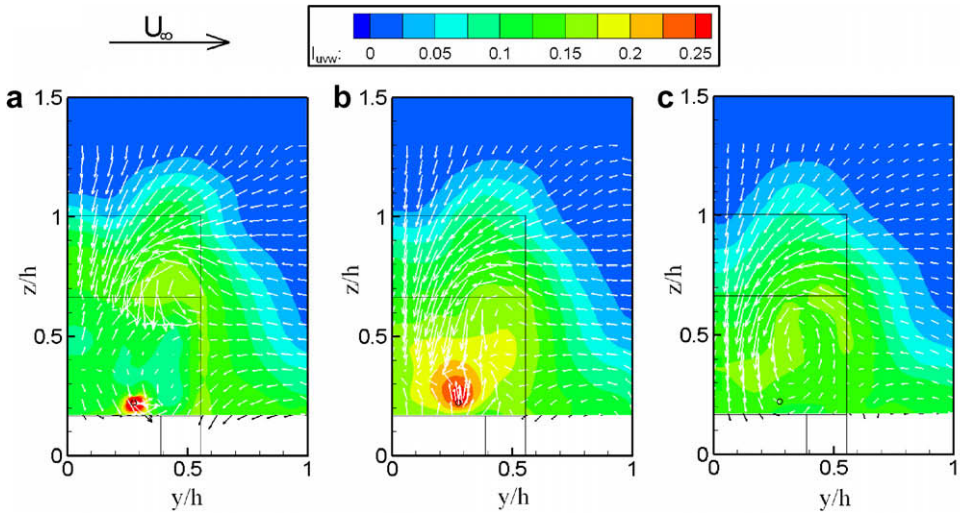

Fig. 12. Turbulence intensity, I_{uvw} contours of the studied model vehicle **A** ($\alpha = 25°$) for $U_j/U_\infty = 4.395$ (a) $x/h = 0.125$, (b) $x/h = 0.5$ and (c) $x/h = 1$.

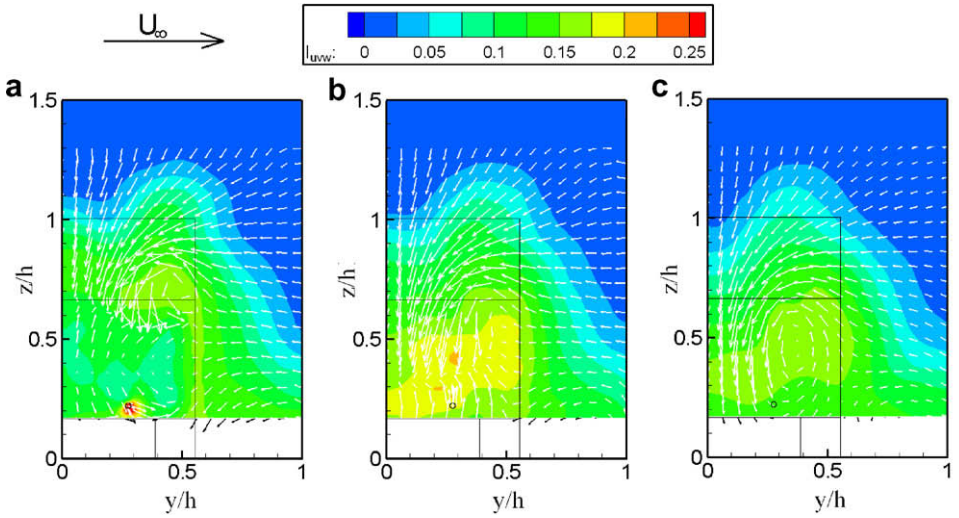

Fig. 13. Turbulence intensity, I_{uvw} contours of the studied model vehicle **A** ($\alpha = 25°$) for $U_j/U_\infty = 1.452$ at (a) $x/h = 0.125$, (b) $x/h = 0.5$ and (c) $x/h = 1$.

studied vehicle wake in order to have a better understanding of the vehicular exhaust pollutant dispersive and mixing natures from a moving vehicle in the wake region. Like previous studies [16,19–22,24,33], the trace gas or hot air (i.e, passive scalar pollutant) from the vehicular exhaust tailpipe was used which is similar to the non-chemical reactive gas characteristics (i.e., carbon monoxide). If only small particles are considered where the Stokes number, St_p is much less than 1, then these particles may be considered to behave like a gas [16,19].

Figs. 14 and 15 show the cross-sectional x–z plane of normalized mean temperature excess, $\overline{T^*}$ (i.e., mean scalar concentration excess) contours and time-averaged flow streamlines for the studied model vehicles **B** and **A**, respectively which is located at the central plane of exhaust tailpipe, $y/h = 0.278$, respectively for two studied driving modes (i.e., 10 km h^{-1} and 30 km h^{-1}). Results show that the heated fluid flow (i.e., scalar concentration) is mainly localized in the lower vortex of the recirculation zone or along the exhaust heated air jet plume for all studied cases. The distribution of the mean temperature field conforms to the streamlines. For low value of the U_j/U_∞, the results are in good agreement with the findings of Richards et al. [19] and their proposed scenario. The hot air jet is neither sent straight to the wake region nor trapped by the recirculation zone. In the latter case, the scalar is drawn by the lower anti-clockwise vortex. Then it goes back to the base of the studied model vehicle **A** and **B** to be trapped by the upper clockwise vortex. For the driving mode of 10 km h^{-1} case of both studied model vehicles, the effect of jet flow exit becomes more predominant. The heated fluid flow follows practically a straight trajectory oriented along the jet exhaust flow in x-axis. Based on the velocity field results as shown in Figs. 6b and 8, the studied model vehicle **A** is more affected by the heated air jet flow. Outside the recirculation zone, the shape of the isotherms is also more stretched for the driving mode of 10 km h^{-1} case whatever the geometry of studied model vehicle is.

Figs. 16 and 17 show the cross-sectional y–z plane of normalized mean temperature excess $\overline{T^*}$ contours and the time-averaged velocity vectors of the studied model vehicle B along the downstream direction at $x/h = 0.125$, 0.5, 1 and 2, respectively. Along the downstream of the exhaust heated air jet flow, the heated fluid flow tends to diffuse the whole recirculation zone, in particular for the driving mode of 30 km h^{-1} case. At $x/h = 0.5$, the maximum values of $\overline{T^*}$ are centered at the front of the vehicular exhaust jet tailpipe exit for the driving mode of 10 km h^{-1} case as shown in Fig. 16b while the maxima zone moves due to the effect of its

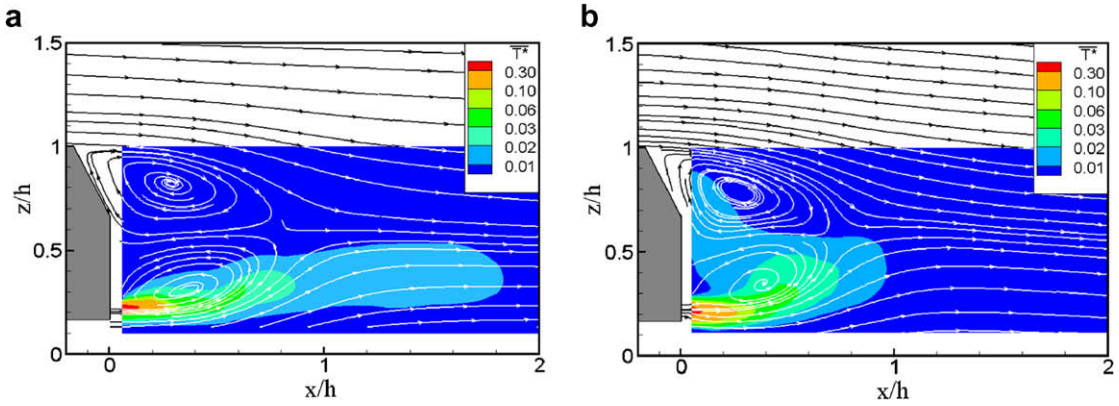

Fig. 14. Normalized mean temperature excess contours $\overline{T^*}$ and time-averaged flow streamlines of the studied model vehicle **B** ($\alpha = 60°$) at $y/h = 0.278$ for (a) $U_j/U_\infty = 2.813$ and (b) $U_j/U_\infty = 0.929$.

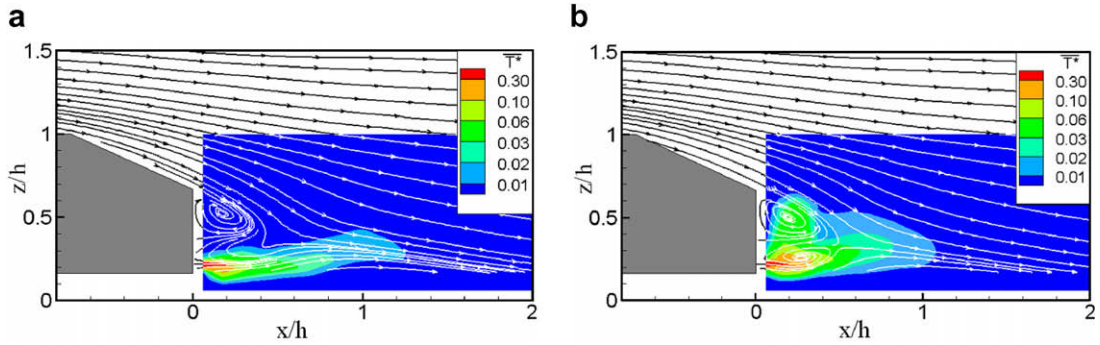

Fig. 15. Normalized mean temperature excess $\overline{T^*}$ contours and time-averaged flow streamlines of the studied model vehicle **A** ($\alpha = 25°$) at $y/h = 0.278$ for (a) $U_j/U_\infty = 4.395$ and (b) $U_j/U_\infty = 1.452$.

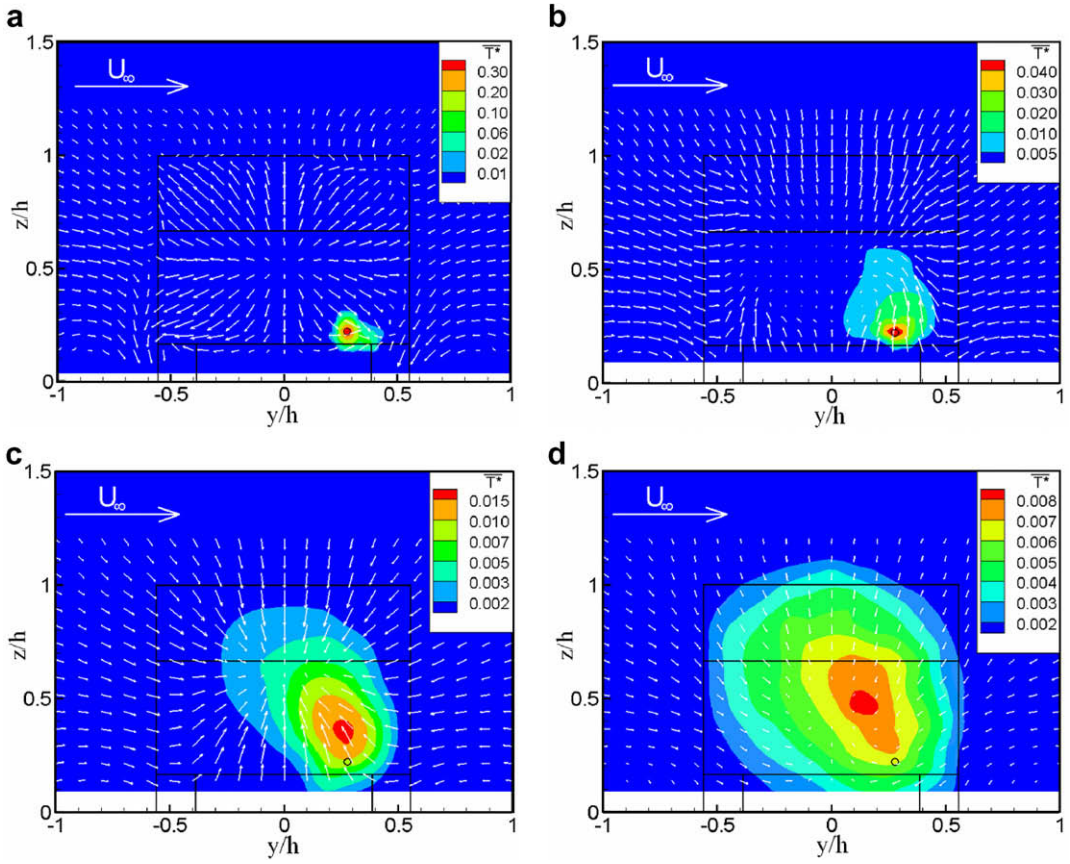

Fig. 16. Normalized mean temperature excess $\overline{T^*}$ contours and time-averaged velocity vectors of the studied model vehicle **B** ($\alpha = 60°$) for $U_j/U_\infty = 2.813$ at (a) $x/h = 0.125$, (b) $x/h = 0.5$, (c) $x/h = 1$ and (d) $x/h = 2$.

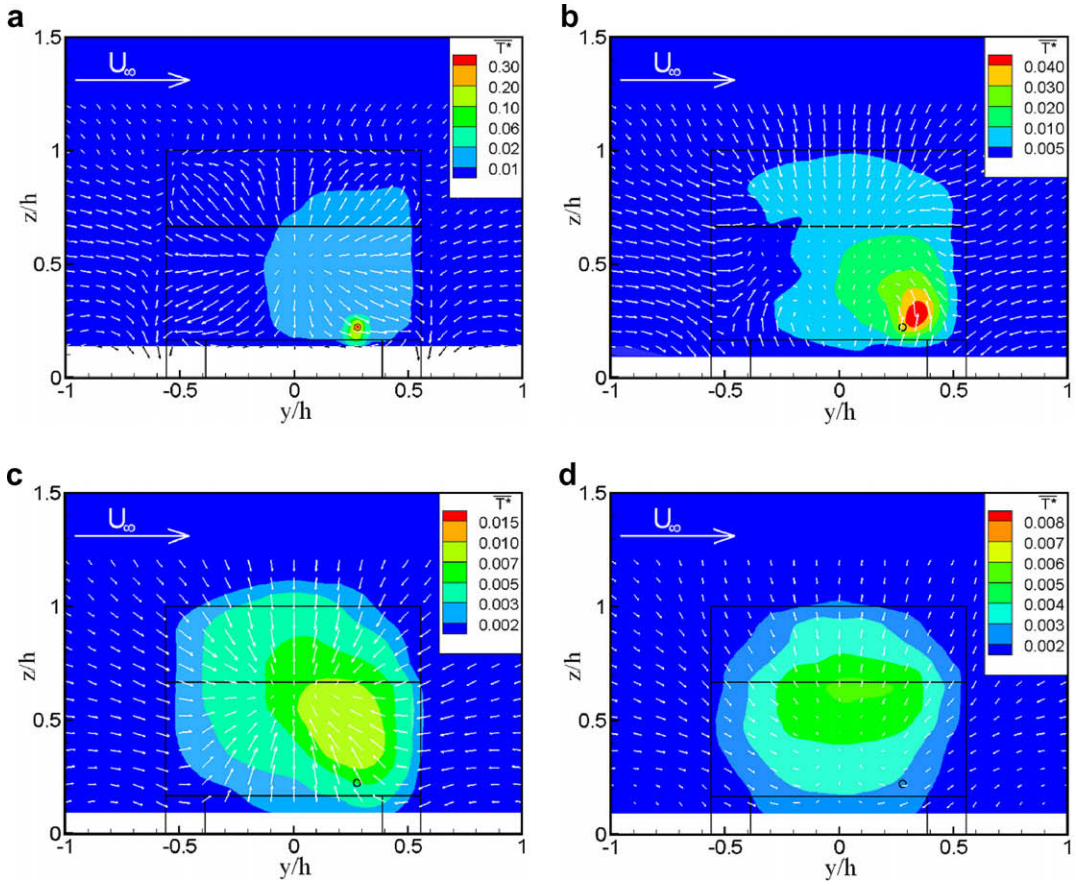

Fig. 17. Normalized mean temperature excess $\overline{T^*}$ contours and time-averaged velocity vectors of the studied model vehicle **B** ($\alpha = 60°$) for $U_j/U_\infty = 0.929$ at (a) $x/h = 0.125$, (b) $x/h = 0.5$, (c) $x/h = 1$ and (d) $x/h = 2$.

lateral flow for the other driving mode of 30 km h^{-1} as shown in Fig. 17b. At $x/h = 1$, outside the recirculation zone, the mean temperature excess field is characterized by a movement to the center of the wake structure for the studied driving modes as shown in Figs. 16c to 17c. At $x/h = 2$, the mean temperature excess field is practically symmetrical to the centerline of the model vehicle B at $y/h = 0$ for the driving mode of 30 km h^{-1} as shown in Fig. 17d. Based on the measured flow fields as shown in Figs. 5, 7 and 9, the velocity field is two-dimensional flow. The temperature field (i.e., scalar concentration field) obtained from the studied model vehicle **B** also confirms the two dimensionality in the near-wake region according to the shape of mean temperature contours as shown in Figs. 16 and 17. This behavior has a good agreement with the previous experimental results of Gosse [16] for an Ahmed reference model with $\alpha = 5°$ and 40° at $Re_h = 6.83 \times 10^3$. Although the value of the Reynolds number used is quite different, the velocity and temperature fields are quite similar from these two experiments.

Figs. 18 and 19 show the cross-sectional y–z plane of normalized mean temperature excess $\overline{T^*}$ contours and the time-averaged velocity vectors of the studied model vehicle **A** along the downstream direction at $x/h = 0.125$, 0.5 and 1, respectively. At $x/h = 0.125$, the different behavior of mean temperature excess fields are observed for the studied driving modes of 10 and 30 km h^{-1}. While the maximum value zone of $\overline{T^*}$ is located at the front of the vehicular exhaust jet tailpipe exit for two studied driving modes of 10 and 30 km h^{-1} cases. The presence of heated fluid flow in the upper vortex of recirculation zone is observed for the studied driving mode of 30 km h^{-1} as shown in Fig. 19. At $x/h = 0.5$, the behavior of the mean temperature field is quite similar whatever the corresponding value of U_j/U_∞ of different driving mode is. At the edge of the bubble zone, the maximum isotherms are stretched in the vertical direction at $x/h = 0.5$, however the maximum isotherms are now located at the edges of the right trailing vortex at $x/h = 1$. Comparing with the temperature fields obtained by Gosse et al. [22], the lower temperature fields (i.e., scalar concentration fields) were measured in the near-wake region of studied model vehicles **A** and **B** for present study. This different behavior may explain by the mass flow rate ratio, $\dot{m}_{\text{hot air}}/\dot{m}_{\text{model vehicle}}$ used in these two experiments. Gosse et al. [22] used $\dot{m}_{\text{hot air}}/\dot{m}_{\text{model vehicle}}$ from 9.78×10^{-3} to 1.73×10^{-2} while the present study used $\dot{m}_{\text{hot air}}/\dot{m}_{\text{model vehicle}}$ from 4.48×10^{-4} to 1.8×10^{-3}.

Comparing with the temperature fields obtained from the studied model vehicle of **B** and **A** as shown in Figs. 16 and 17, and Figs. 18 and 19, respectively, the results show that the shape of mean temperature field (i.e. scalar concentration field) contours depend mainly on the effect of the exit jet condition. On the contrary, for the studied model vehicle of $\alpha = 25°$, the three dimensional wake structure is characterized by the two longitudinal vortices and the effect of vehicular exhaust jet flow is minimized. The right trailing vortex has drawn the heat fluid flow on its side of the studied vehicle **A** while the left one has drawn the clean air. The main consequence is to decrease significantly the temperature level for the two studied driving modes (i.e., 10 and 30 km h^{-1}) when $x/h > 1$. This behavior has a good agreement with the findings of Gosse et al. [22] and Eskridge and Rao [33].

Fig. 20 shows the maximum values of normalized temperature intensity $I_{T'_{\max}}$ (i.e., normalized scalar concentration intensity) along the longitudinal direction of the studied model vehicles **A** and **B** for different driving modes. Similar behavior of longitudinal direction

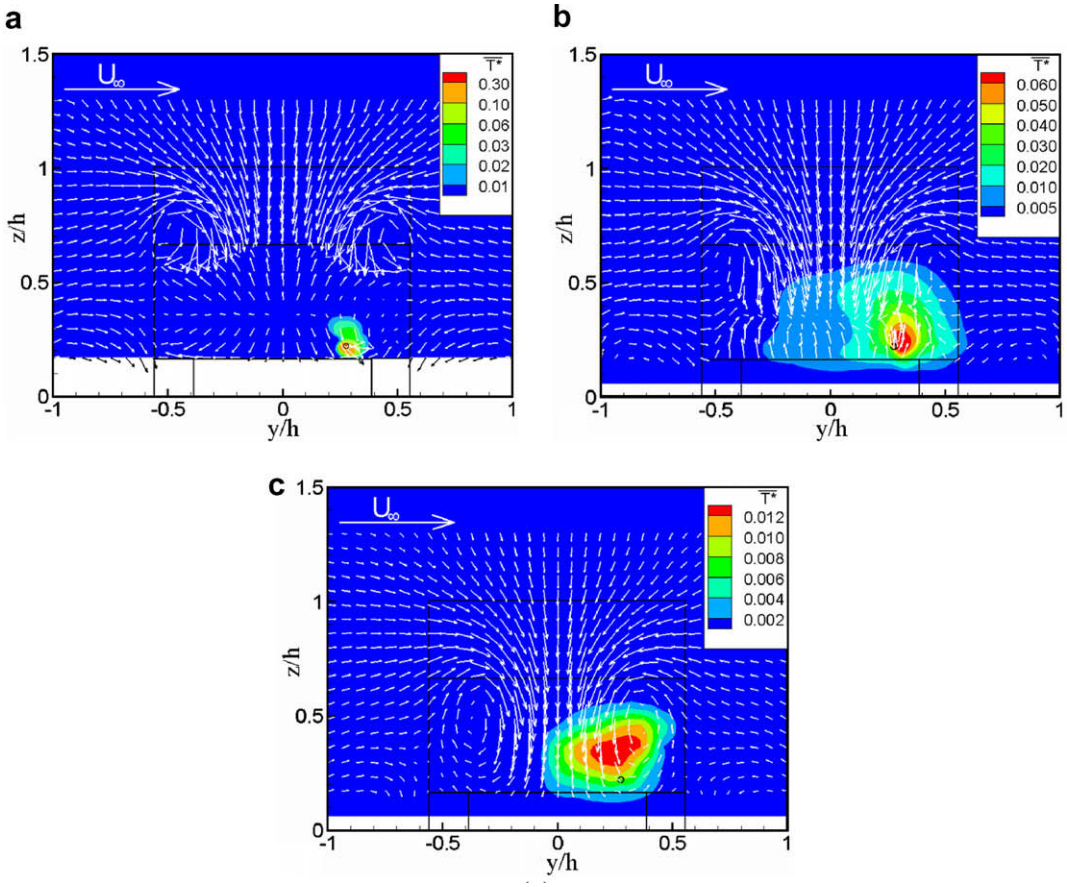

Fig. 18. Normalized mean temperature excess $\overline{T^*}$ contours and time-averaged velocity vectors of the studied model vehicle **A** ($\alpha = 25°$) for $U_j/U_\infty = 4.395$ at (a) $x/h = 0.125$, (b) $x/h = 0.5$ and $x/h = 1$.

of $I_{T'_{max}}$ is observed for whatever the effect of rear slant angle of studied model vehicles and U_j/U_∞ for different driving modes except the studied model vehicle **A** for the driving mode of 10 km h^{-1}. The values of $I_{T'_{max}}$ reach their maximum from 0.59 to 0.77 at $x/h = 0.5$, and then decrease their $I_{T'_{max}}$ values along the downstream of the two studied model vehicles **A** and **B** for driving modes of 30 to 70 km h^{-1} except the studied model vehicle **A** for the driving mode of 10 km h^{-1} case. On the contrary, the results show that a high value of $I_{T'_{max}}$ is located to the closest of the injection zone and a low value of $I_{T'_{max}}$ at $x/h = 0.5$ for the studied model vehicle **A** and the driving mode of 10 km h^{-1} case when comparing with the other driving mode cases. In the first case, the driving mode for the studied model vehicle **A** is 10 km h^{-1} at $x/h = 0.125$, the results could be explained by its high value of the turbulent flow intensity I_{uvw} at this point (i.e., $I_{uvw,\ max} = 0.6$). In the second case, where the driving mode for the studied vehicle **A** is 10 km h^{-1} at $x/h = 0.5$, this low value of $I_{T'_{max}}$ is related to the high level of the mean temperature $\overline{T^*}$ (i.e., mean scalar concentration). On the other hand, the results of temperature intensity (i.e., scalar concentration intensity) reveal the effect of the longitudinal vortices on the scalar dispersion in particular at $x/h = 1$. For the studied model vehicles **B** and **A**, the values of $I_{T'_{max}}$ are bounded between $0.632 \leqslant I_{T'_{max}} \leqslant 0.723$ and $0.328 \leqslant I_{T'_{max}} \leqslant 0.485$, respectively. Comparing with two studied rear slant angles, the levels of $I_{T'_{max}}$ are two times higher for $\alpha = 60°$ (vehicle **B**) than $\alpha = 25°$ (vehicle **A**) case except for the driving mode of 10 km h^{-1}. The different levels of $I_{T'_{max}}$ are due to the presence of the trailing vortex at the vehicular exhaust jet side of the studied model vehicle **B**. In Figs. 18 and 19, the heated fluid flow (i.e., scalar concentration) is trapped by the longitudinal vortex. This phenomenon seems to have a consequence on the levels of $\overline{T'^{*2}_{max}}^{1/2}$ (i.e., normalized maximum standard deviation of the scalar concentration). Comparing with the two studied rear slant angles, the values of $\overline{T'^{*2}_{max}}^{1/2}$ for the studied model vehicle **A** ($\alpha = 25°$) are about two times smaller than for the studied model vehicle **B** ($\alpha = 60°$) whatever the driving modes are. For the studied model vehicles **B** and **A**, the values of $\overline{T'^{*2}_{max}}^{1/2}$ are bounded about $5.89 \times 10^{-3} \leqslant \overline{T'^{*2}_{max}}^{1/2} \leqslant 11.7 \times 10^{-3}$ and $3.28 \times 10^{-3} \leqslant \overline{T'^{*2}_{max}}^{1/2} \leqslant 6.33 \times 10^{-3}$, respectively.

4. Conclusion

Experimental investigations of the interaction effect of rear slant angle (i.e., $\alpha = 25°$ and 60°) and heated air exhaust jet condition (i.e., U_j and T_j) on flow structures, and pollutant (i.e., scalar) dispersion and concentration fields in the near-wake region of two simplified scale-model vehicles at Reynolds number $Re_h = 5.8 \times 10^4$ were performed in a closed-circuit wind tunnel using laser Doppler anemometry (LDA) and the cold wire thermometry. The results show that the behaviors of flow structures and pollutant dispersion in the near-wake region of the studied model vehicles are highly dependent on the interaction effect of U_j/U_∞ and α. For the low value of U_j/U_∞ (i.e., the driving mode from 30 km h^{-1} to 70 km h^{-1}), the wake structure of the both studied model vehicles is almost similar to the case without introducing the vehicular exhaust jet flow, $U_j/U_\infty = 0$, but the scalar concentration is neither sent straight to the wake region nor trapped by the recirculation zone. For higher value of U_j/U_∞ (i.e., the driving mode of 10 km h^{-1}), the jet flow perturbation along the central plane of the vehicular exhaust tailpipe causes the disappearance of the low-

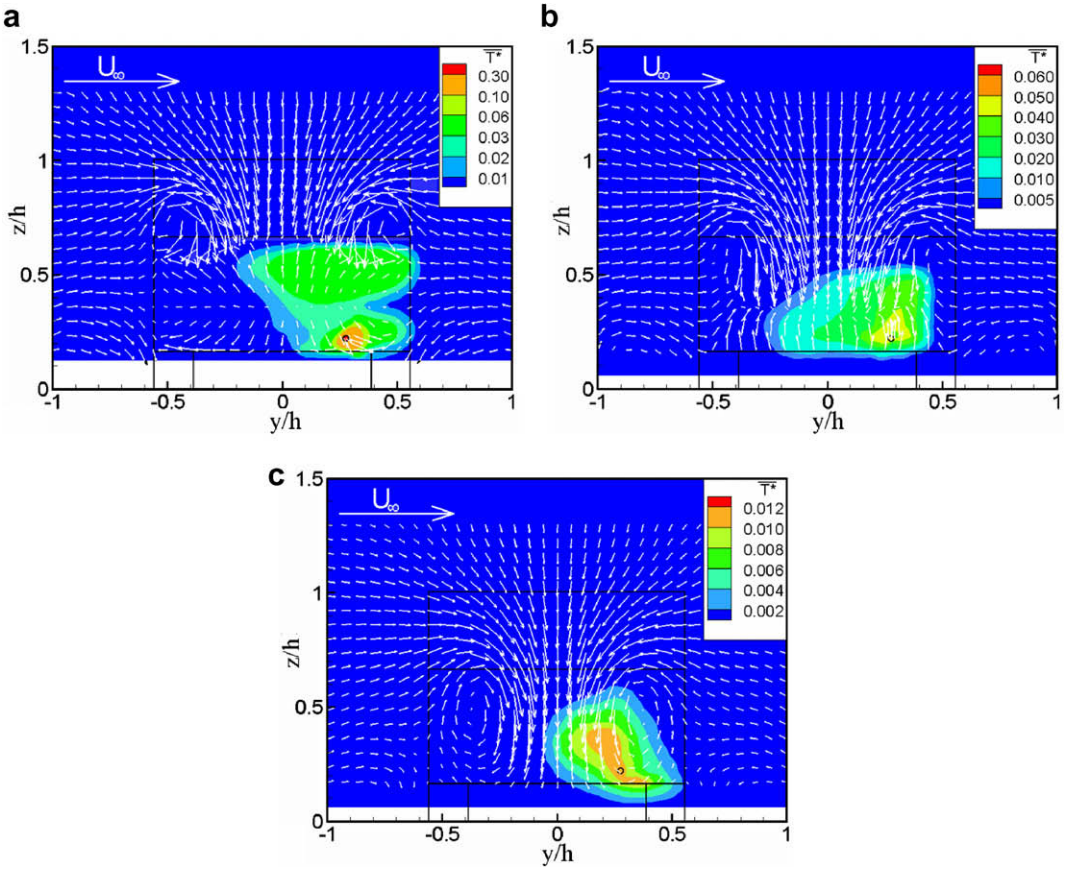

Fig. 19. Normalized mean temperature excess $\overline{T^*}$ contours and time-averaged velocity vectors of the studied model vehicle **A** ($\alpha = 25°$) for $U_j/U_\infty = 1.452$ at (a) $x/h = 0.125$, (b) $x/h = 0.5$ and (c) $x/h = 1$.

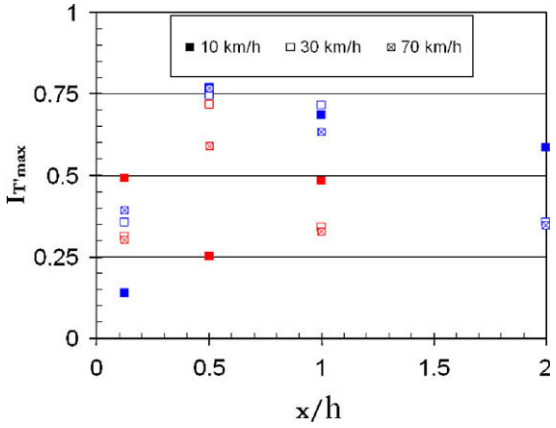

Fig. 20. The maximum values of normalized temperature intensity $I_{T'_{max}}$ along the longitudinal direction of the studied model vehicles **A** (in red) and **B** (in blue) for different driving modes.

er vortex in the recirculation zone for the studied model vehicle **A** ($\alpha = 25°$) while it causes the stretching of the recirculation zone for the studied model vehicle **B** ($\alpha = 60°$). The contaminant is mainly straight trajectory along its jet exhaust flow axis. Outside the recirculation zone, the flow field becomes symmetrical and its flow structure depends only on the rear slant angle of the studied model vehicle. The scalar concentration field of the studied model vehicle **B** is characterized by a two-dimensional flow structure whatever the studied driving modes are. The distribution of the mean normalized temperature excess field (i.e., scalar concentration field) conforms to the velocity vector field for both studied model vehicles. For the studied model vehicle **A**, the scalar concentration is drawn to the edge of the trailing vortex at the vehicular exhaust jet side. This phenomenon causes a significant reduction of the scalar concentration level whatever the studied driving modes are.

Acknowledgements

This work was supported by the Grants from the Research Grants Council of the Hong Kong Special Administrative Region, China (Project No. PolyU 5265/04E), and Central Research Grants and the research studentship of The Hong Kong Polytechnic University (Project Nos. B-Q853 and G-YF29).

References

[1] H. Mayer, Air pollution in cities, Atmos. Environ. 33 (24–25) (1999) 4029–4037.
[2] P. Sharma, M. Khare, Modelling of vehicular exhausts – a review, Trans. Res. Part D-Trans. Environ. 6 (3) (2001) 179–198.
[3] T.L. Chan, G. Dong, C.W. Leung, C.S. Cheung, W.T. Hung, Validation of a two-dimensional pollutant dispersion model in an isolated street canyon, Atmos. Environ. 36 (5) (2002) 861–872.
[4] X.X. Li, C.H. Liu, D.Y.C. Leung, K.M. Lam, Recent progress in CFD modelling of wind field and pollutant transport in street canyons, Atmos. Environ. 40 (29) (2006) 5640–5658.
[5] J.S. Wang, T.L. Chan, Z. Ning, C.W. Leung, C.S. Cheung, W.T. Hung, Roadside measurement and prediction of CO and $PM_{2.5}$ dispersion from on-road vehicles in Hong Kong, Trans. Res. Part D-Trans. Environ. 11 (4) (2006) 242–249.
[6] S. Weber, W. Kuttler, K. Weber, Flow characteristics and particle mass and number concentration variability within a busy urban street canyon, Atmos. Environ. 40 (39) (2006) 7565–7578.
[7] S.D. Shah, K.C. Johnson, J.W. Miller, D.R. Cocker, Emission rates of regulated pollutants from on-road heavy-duty diesel vehicles, Atmos. Environ. 40 (1) (2006) 147–153.

[8] T.L. Chan, Z. Ning, J.S. Wang, C.S. Cheung, C.W. Leung, W.T. Hung, Gaseous and particle emission factors from the selected on-road petrol/gasoline, diesel and liquefied petroleum gas vehicles, Energy Fuels 21 (5) (2007) 2710–2718.
[9] L. Gidhagen, C. Johansson, J. Langner, G. Olivares, Simulation of NOx and ultrafine particles in a street canyon in Stockholm, Sweden, Atmos. Environ. 38 (14) (2004) 2029–2044.
[10] T.L. Chan, K. Zhou, L.Z. Lin, Modelling study of gas-to-nanoparticle conversion from a vehicular exhaust jet plume, in: International Conference on Jets, Wakes and Separated Flows, ICJWSF-2005 October 5–8, 2005, Toba-shi, Mie, Japan.
[11] R. Paoli, F. Garnier, Interaction of exhaust jets and aircraft wake vortices: small-scale dynamics and potential microphysical–chemical transformations, C.R. Phys. 6 (4–5) (2005) 525–547.
[12] T. L Chan, J.Z. Lin, K. Zhou, C.K. Chan, Simultaneous numerical simulation of nano and fine particle coagulation and dispersion in a round jet, J. Aerosol Sci. 37 (11) (2006) 1545–1561.
[13] J.Z. Lin, T.L. Chan, S. Liu, K. Zhou, Y. Zhou, S.C. Lee, Effects of coherent structures on nanoparticle coagulation and dispersion in a round jet, Int. J. Nonlinear Sci. Numer. Simulat. 8 (1) (2007) 45–54.
[14] Z.Q. Yin, J.Z. Lin, K. Zhou, T.L. Chan, Numerical simulation of the formation of pollutant nanoparticles in the exhaust twin-jet plume of a moving car, Int. J. Nonlinear Sci. Numer. Simulat. 8 (4) (2007) 535–543.
[15] T.L. Chan, G. Dong, C.S. Cheung, C.W. Leung, C.P. Wong, W.T. Hung, Monte Carlo simulation of nitrogen oxides dispersion from a vehicular exhaust plume and its sensitivity studies, Atmos. Environ. 35 (35) (2001) 6117–6127.
[16] K. Gosse, Etude expérimentale de la dispersion d'un scalaire passif dans le proche sillage d'un corps d'ahmed, Thèse Sc. Phys. (Ph.D.), Université de Rouen, France, November 2005.
[17] J.S. Wang, T.L. Chan, C.S. Cheung, C.W. Leung, W.T. Hung, Three-dimensional pollutant concentration dispersion of a vehicular exhaust plume in the real atmosphere, Atmos. Environ. 40 (3) (2006) 484–497.
[18] A. Venkatram, D. Fitz, K. Bumiller, S. Du, M. Boeck, C. Ganguly, Using a dispersion model to estimate emission rates of particulate matter from paved road, Atmos. Environ. 33 (7) (1999) 1093–1102.
[19] K.A. Richards, N.G. Wright, C.J. Baker, A.J. Baxendale, Computational modelling of pollution dispersion in the near wake of a vehicle, in: International Conference on Aerodynamics, Proceedings of the MIRA, Rugby, UK, 2000.
[20] G. Dong, T.L. Chan, Large eddy simulation of flow structures and pollutant dispersion in the near-wake region of a light-duty diesel vehicle, Atmos. Environ. 40 (6) (2006) 1104–1116.
[21] T.L. Chan, D.D. Luo, C.S. Cheung, C.K. Chan, Large Eddy simulation of flow structures and pollutant dispersion in the near-wake region of the studied ground vehicle for different driving conditions, Atmos. Environ. 42 (21) (2008) 5317–5339.
[22] K. Gosse, P. Paranthoën, B. Patte-Rouland, M. Gonzalez, Dispersion in the near wake of idealized car model, Int. J. Heat Mass Transfer 49 (9-10) (2006) 1747–1752.
[23] S.R. Ahmed, R. Ramm, G. Faltin, Some salient features of the time-averaged ground vehicle wake. SAE Technical Paper No. 840300, USA, 1984.
[24] I. Kanda, K. Uehara, Y. Yamao, Y. Yoshikawa, T. Morikawa, A wind tunnel study on exhaust gas dispersion from road vehicles – Part I: velocity and concentration fields behind single vehicles, J. Wind Eng. Ind. Aerodyn. 94 (9) (2006) 639–658.
[25] R. Narasimha, S.N. Prasad, Leading edge shape for flat plate boundary layer studies, Exp. Fluids 17 (5) (1994) 358–360.
[26] J.F. Huang, T.L. Chan, Y. Zhou, Boundary layer thickness and root mean square values of the designed flat plate, Internal Technical Report, Department of Mechanical Engineering, The Hong Kong Polytechnic University, Hong Kong, 2007.
[27] T.L. Chan, C.W. Leung, K. Jambunathan, S. Ashforth-Frost, Y. Zhou, M.H. Liu, Heat transfer characteristics of a slot jet impinging on a semi-circular convex surface, Int. J. Heat Mass Transfer 45 (5) (2002) 993–1006.
[28] C.M. Silva, M. Costa, T.L. Farias, H. Santos, Evaluation of SI engine exhaust gas emissions upstream and downstream of the catalytic converter, Energy Convers. Manage. 47 (18–19) (2006) 2811–2828.
[29] T.L. Chan, Y. Zhou, M.H. Liu, C.W. Leung, Mean flow and turbulence measurements of the impingement wall jet on a semi-circular convex surface, Exp. Fluids 34 (1) (2003) 140–149.
[30] S.R. Ahmed, Influence of base slant on wake structure and drag of road vehicles, ASME J. Fluids Eng. 105 (1983) 429–434.
[31] H. Lienhart, S. Becker, Flow and turbulence structures in the wake of a simplified car model, SAE Technical Paper No.: 2003-01-0656, USA, 2003.
[32] R.M. Pagliarella, S. Watkins, A. Tempia, The effect of rear slant angle on vehicle wakes and implications for platoons. SAE Technical Paper No.: 2006-01-0341, USA.
[33] R.E. Eskridge, S.T. Rao, Turbulent–diffusion behind vehicles: experimentally determined turbulence mixing parameters, Atmos. Environ. 20 (5) (1986) 851–860.